Journal Name

ARTICLE

Electrical conductivity and conduction mechanisms in $(Na_{0.5}Bi_{0.5}TiO_3)_{1-x}(BiScO_3)x$ (0.00 ≤ x ≤ 0.25) solid solutions

Received 00th January 20xx,
Accepted 00th January 20xx

DOI: 10.1039/x0xx00000x

www.rsc.org/

F. Yang,[a,] † P. Wu[a] and D. C. Sinclair[a,] †

The electrical properties of $(Na_{0.5}Bi_{0.5}TiO_3)_{1-x}(BiScO_3)_x$ (NBT-BS, 0.00 ≤ x ≤ 0.25) solid solutions are established by ac impedance spectroscopy and electromotive force transport number measurements. The bulk conductivity decreases with increasing BS incorporation but the oxide-ion transport number remains high (> 0.85) over a wide compositional range 0.00 ≤ x ≤ 0.15 and drops to ~ 0.7 for x ≥ 0.20. NBT-BS solid solutions can only present either predominant oxide-ion conduction or mixed ionic-electronic conduction behaviour, indicating that oxide-ion conduction cannot be fully eliminated by incorporation of BS. This is in contrast from our previous study that incorporation of ~7% $BiAlO_3$ (BA) can fully suppress the oxide-ion conduction in NBT. The conductivity-composition relationships of NBT-BS solid solutions are attributed to a competing effect from lattice expansion, which enlarges the channel for oxygen ion migration, with trapping between B-site acceptor ions, Sc'_{Ti}, and oxygen vacancies, $V_O^{\bullet\bullet}$, which decreases oxygen ion migration. Comparisons between NBT-BS, NBT-BA and NBT-$BiGaO_3$ (BG) solid solutions suggest that small acceptor ions on the B-site are more effective in trapping oxygen vacancies and consequently more effective to suppress the oxide-ion conduction and thus reduce dielectric loss at elevated temperatures.

Introduction

Sodium bismuth titanate, $Na_{0.5}Bi_{0.5}TiO_3$, is one of the most promising lead-free piezoelectric materials for piezoelectric[1, 2] and dielectric[3, 4] applications. It can also be an excellent oxide-ion conductor and therefore a potential electrolyte material for intermediate-temperature solid oxide fuel cells (IT-SOFCs).[5] Because of its potential application in such technologically importance devices, NBT has been receiving increasing attention and numerous efforts to modify its properties by defect chemistry design have been undertaken.[6]

The potential variety of applications for NBT is attributed to its diverse range of electrical properties. In a previous study,[7] we proposed that NBT can present three types of electrical behaviour, which can be distinguished by their electrical conduction mechanism(s), magnitude of bulk conductivity (σ_b), oxide-ion transport number (t_{ion}) and dielectric loss – temperature (tan δ – T, at 1 MHz) profile according to

i) Type I, predominant oxide-ion conduction mechanism, high σ_b (> 10^{-3} S cm^{-1} at 600 °C), t_{ion} > 0.85, sharp increase of tan δ with increasing temperature and tan δ exceeds 0.2 at ~ 350 °C.
ii) Type II, mixed electronic-ionic conduction mechanism, intermediate σ_b (10^{-6} - 10^{-3} S cm^{-1} at 600 °C), 0.15 < t_{ion} < 0.85, low tan δ in a narrow temperature range and a steep rise above ~ 500 °C to exceed 0.1 at 600 °C.
iii) Type III, predominant electronic conduction mechanism, very low σ_b (~ 10^{-6} S cm^{-1} at 600 °C), t_{ion} < 0.15, low tan δ over a wide temperature range (< 0.02 from 300 to 600 °C).

The electrical properties of NBT can be flexibly tuned among Types I, II and III by various defect mechanisms including

i) A-site Bi non-stoichiometry.[7, 8] Nominally stoichiometric NBT ($NB_{0.50}T$), under our processing conditions, is an oxide-ion conductor. The high ionic conductivity in $NB_{0.50}T$ is attributed to oxygen vacancies generated by low levels of Bi_2O_3 loss during ceramic processing, as well as the high oxygen ion mobility associated with highly polarised Bi^{3+} ions and weak Bi-O bonds.[2] Bi-deficient NBT, i.e., $Na_{0.50}Bi_{0.49}TiO_{2.985}$ ($NB_{0.49}T$), has higher oxide-ion conductivity due to creation of additional oxygen vacancies this increasing the charge carrier concentration. $NB_{0.50}T$ and $NB_{0.49}T$ show typical Type I behaviour. On the contrary, Bi-excess NBT, i.e., $Na_{0.50}Bi_{0.51}TiO_{3.015}$ ($NB_{0.51}T$), shows very low conductivity with t_{ion} < 0.1. Impedance measurements under various pO_2, and ^{18}O tracer diffusion measurements confirmed $NB_{0.51}T$ to exhibit an *n*-type electronic conduction mechanism[2] and shows Type III behaviour. A further increase in the Bi-excess content, i.e., $Na_{0.50}Bi_{0.52}TiO_{3.03}$ ($NB_{0.52}T$), shows a mixed electronic-ionic conduction mechanism with t_{ion} ~ 0.5, and presents type II behaviour. Re-introduction of oxide-ion conduction in $NB_{0.52}T$ may be related to a compositional change in the NBT-phase due to the presence of a Bi-rich secondary phase or a space charge effect. An increase in the starting Bi content in NBT, from $NB_{0.49}T$ to $NB_{0.52}T$, can change the electrical behaviour of NBT in the sequence of Type I → III → II.
ii) B-site donor doping.[7] Nb-doping on B-site of $NB_{0.50}T$, i.e., $Na_{0.50}Bi_{0.50}Ti_{1-x}Nb_xO_{3+0.5x}$, can fill in the oxygen vacancies in $NB_{0.50}T$ according to

$$Nb_2O_5 + 2Ti_{Ti}^x + V_O^{\bullet\bullet} \rightarrow 2Nb_{Ti}^{\bullet} + TiO_2 + O_O^x, \quad (1)$$

and consequently supresses the oxide-ion conduction in NBT to change the electrical conduction mechanism from oxide-ion

[a] Department of Materials Science & Engineering, University of Sheffield, Mappin Street, Sheffield, S1 3JD, United Kingdom.
† Corresponding authors. fan.yang@sheffield.ac.uk; d.c.sinclair@sheffield.ac.uk

conduction for x = 0, to mixed electronic-electronic conduction for x = 0.002 and 0.003 and finally to *n*-type electronic conduction for $x \geq 0.02$. In this case, the electrical behaviour of NBT changes in the sequence of Type I → II → III with increasing B-site donor doping level.

iii) Solid solution with some Bi-based high pressure perovskites. A recent study[9] found that incorporation of $BiAlO_3$ (BA) into $NB_{0.50}T$ can suppress the oxide-ion conduction and change the conduction mechanism with increasing BA level from oxide-ion conduction (type I) to mixed ionic-electronic conduction (type II) and finally to electronic conduction (type III). The suppression of oxide-ion conduction with increasing BA content was attributed mainly to a decrease in oxygen vacancy mobility associated with trapping between negatively charged acceptor dopants Al'_{Ti} and positively charged oxygen vacancies $V_O^{\bullet\bullet}$. This provides an alternative approach to fine-tune the electrical conduction behaviour of NBT following the sequence of Type I → II → III. It is found that ~ 7% BA can fully suppress the oxide-ion conduction in $NB_{0.50}T$ and therefore significantly reduce the dielectric loss at elevated temperatures to make it an excellent high-temperature dielectric material. A similar effect is also observed in NBT-$BiGaO_3$ (BG) solid solutions.

The above studies suggest that tuning of the electrical properties is fulfilled by controlling the oxide-ion conduction in NBT, i.e., by varying the concentration and/or mobility of oxygen vacancies. Therefore, it is important to establish further understanding of the factors that are critical to the oxygen ion migration in NBT. Previous modelling studies[10-12] show the local configurations of Na and Bi ions on the A-site play an important role and a Bi-rich environment is beneficial for oxide-ion conduction in NBT because it provides the lowest energy barrier for oxygen ion migration. Experimentally it is found that, at the same nominal oxygen vacancy concentration, NBTs with B-site acceptor dopants usually present lower oxide-ion conductivity than those with A-site acceptor dopants,[6] indicating a tendency for trapping of oxygen vacancies by B-site acceptor dopants, which is also proposed by first-principles studies.[12-14] However, acceptor-doping on B-sites generates oxygen vacancies, which increases the charge carrier concentration but the solid solution limit of B-site acceptor dopants in NBT is usually rather low (typically < 2%). As a consequence, it is difficult to differentiate the possible effects from various B-site acceptor dopant ions, e.g, size, polarisability, bond strength with oxygen, etc. on the oxide-ion conductivity.

To increase the B-site acceptor dopant level without generating additional oxygen vacancies, Bi-based high-pressure phases such as $BiAlO_3$ and $BiGaO_3$ have been used to form solid solutions with NBT; however, they only expand the acceptor dopant concentration on the B-site to ~ 6% (based on SEM).[9] Compared to BA and BG, $BiScO_3$ (BS) has a much higher solid solution limit (~ 25%) in NBT and its effect on the crystal structure and dielectric properties on NBT has been investigated. Marchet *et al.*[15] and Boucher *et al.*[16] reported an increased Curie temperature as well as a higher degree of diffuseness in the phase transition due to the disorder in the cationic sublattice caused by substitution of Ti by Sc. Nagata and Takenaka[17] studied the dielectric and piezoelectric properties of NBT-BS solid solutions and proposed these ceramics are good candidates as lead-free piezoelectrics. These studies focused mainly on the dielectric/piezoelectric properties without considering the electrical conduction mechanism(s), which are critical to the dielectric loss and leakage current of NBT-based materials.

The NBT-BS solid solution provides a good system to understand the critical factors that influence the oxide-ion conduction in NBT-based materials. First, as the ionic radius of Sc^{3+} (0.745 Å, 6-fold coordination)[18] is much larger than Ti^{4+} (0.605 Å, 6-fold coordination)[18], and the ionic radii of Na^+ and Bi^{3+} are very similar[19] (1.39 Å, 12-fold coordination)[18], high levels of BS into NBT can substantially expand the cell volume, which may provide valuable information on the effect of average structure such as the specific free volume V_{sf},[20] and critical radius r_C[21] on the oxygen ion migration. Second, high levels of BS into NBT may make it possible to further investigate the trapping effect between B-site acceptor dopants and oxygen vacancies. Furthermore, comparing the electrical properties of NBT-BS solid solutions with the previously reported properties for NBT-BA and -BG solid solutions will highlight the importance of ionic size of the B-site dopants on the conductivity and conduction mechanism of NBT.

Here, the electrical conductivity and conduction mechanism of NBT-BS solid solutions are studied by impedance spectroscopy and electromotive force transport number measurements. The purpose of this study is to further understand the factors that control the oxide-ion conduction in NBT to tailor its electrical properties according to requirements for various applications. The results show BS incorporation decreases the bulk conductivity of NBT but it cannot fully eliminate the oxide-ion conduction. Even at the upper solid solution limit (25%), NBT-BS still shows an ionic transport number of ~ 0.7, which is very different from our previous study where ~7% $BiAlO_3$ (BA) incorporation can fully suppress the oxide-ion conduction in NBT. Within the solid solution limit, NBT-BS solid solutions can present only either Type I (predominant oxide-ion conduction) or Type II (mixed ionic-electronic conduction) behaviour. Comparisons between NBT-BS, NBT-BA and NBT-BG solid solutions suggest that large acceptor ions on the B-site are less effective in trapping oxygen vacancies and consequently less effective in suppressing the oxide-ion conduction and reducing the dielectric loss at elevated temperatures.

Experimental

$(Na_{0.5}Bi_{0.5}TiO_3)_{1-x}(BiScO_3)_x$ ($0.00 \leq x \leq 0.25$) solid solutions were prepared by a solid state reaction method using Na_2CO_3 (99.5%, Fisher chemical, UK), Bi_2O_3 (99.9%, Acros Organics, USA), TiO_2 (99.9%, Sigma Aldrich, UK) and Sc_2O_3 (99.9%, Stanford Advanced Materials, USA) as starting materials. Prior to weighing, the raw powders were dried overnight at 300 °C for Na_2CO_3 and Bi_2O_3 and 900 °C for TiO_2 and Sc_2O_3. Appropriate amounts of each precursor were weighed and mixed thoroughly in iso-propanol using yttria-stabilised zirconia grinding media for 6 h. The mixture was dried at 85 °C overnight, sieved and calcined at 850 °C for 2 h. The resultant powder was subjected to a second round of ball milling, drying, sieving and then calcined at 950 °C for 2 h. After a third round of milling, drying and sieving, the final powder was compacted into pellets by uni-axial cold pressing followed by isostatic pressing at 200 MPa. Pellets were embedded in sacrificial powder of the same composition and sintered in air for 2 h at 1200 °C for $0.02 \leq x \leq 0.15$ and 1150 °C for x = 0.00, 0.20 and 0.25 to obtain dense ceramics. After sintering,

pellets were ground using SiC sand paper to remove the sacrificial powder. Pellets ~ 0.85 cm in diameter and ~ 0.15 cm in thickness were used for impedance and LCR measurements.

Ceramic density was measured by the Archimedes' method and compared to the theoretical X-ray density. Phase purity was examined by X-ray diffraction on crushed pellets using a high-resolution STOE STADI-P diffractometer (STOE & Cie GmbH, Darmstadt, Germany) operating with CuKα_1 radiation with a linear position-sensitive detector. Before measurements, the crushed pellets were annealed at 400 °C for 4 h to eliminate any residual stress caused by crushing and grinding. Structural refinement was carried out for reflections in the range of 20° ≤ 2θ ≤ 100° using EXPGUI.[22, 23] Ceramic microstructures were observed by scanning electron microscopy on thermally-etched surfaces using a Philips XL30 SEM. Compositions were obtained by energy dispersive X-ray spectroscopy (EDS) on carbon-coated polished surfaces (without thermal etching).

Electrical properties of the pellets were obtained from ac impedance spectroscopy using an Agilent E4980A impedance analyser (Agilent Technologies Inc., Palo-Alto, CA; frequency range 1 MHz to 20 Hz) and/or a Solartron 1260 system (Solartron Analytical, UK; frequency range 1 MHz to 0.01 Hz). Before measurements, Au paste was painted to cover both surfaces of the pellets and then fired at 850 °C for 2 h to serve as electrodes. Equivalent circuit fitting was performed using ZView software (Scribner Associates, Inc, Southern Pines, NC). Dielectric properties were measured using an LCR meter (Agilent E4980 Precision LCR Meter, Agilent Technologies) with an applied ac voltage of 100 mV. Data points were collected every 60 s from room temperature (RT) to 800 °C using a non-inductively wound tube furnace at a ramping rate of 1 °C min^{-1}. Oxygen-ion transport number measurements were performed using a Probostat system (NorECs Norwegian Electro Ceramics AS, Oslo, Norway). A sample, ~ 1.7 cm in diameter and ~ 0.2 cm in thickness, was sealed onto an YSZ tube using a commercial glass frit. Before that, Pt electrodes, ~ 1.0 cm in diameter, were coated in the centre of the pellet surfaces and fired at 900 °C for 2 h. An oxygen partial pressure (pO_2) difference was created across the ceramic by flowing N_2 into the YSZ tube and leaving the outside of the ceramic in air. The pO_2 difference was monitored by measuring the voltage across the inner and outer electrodes on the YSZ tube. The voltage was measured using a Keithley 182 sensitive digital voltmeter.

Results

$(NBT)_{1-x}(BS)_x$ ($0.00 \le x \le 0.25$) solid solutions are phase-pure based on XRD (Fig.1a). The superlattice reflection from a rhombohedral structure, as shown by the expanded view of the 2θ range between 37 and 43° (Fig.1b), can be observed for all compositions and its intensity decreases with increasing *x*. No (002) and (200) peak splitting from the tetragonal structure is observed in the 2θ range between 45 and 49° (Fig.1c). The above information suggests the structure of $(NBT)_{1-x}(BS)_x$ ($0.00 \le x \le 0.25$) solid solutions could be refined to a rhombohedral cell (space group *R3c*, Fig.1d, x = 0.20 as an example). The lattice parameters, both *a* and *c*, as well as the cell volume increases with increasing *x* (Fig.1e). The relative density of sintered ceramics was ~ 95%, as listed in Table 1.

A typical SEM micrograph of a thermally-etched surface of a solid solution is shown in Fig.2a. Average grain sizes of the solid solutions are 8 – 10 μm for x = 0.00 and 0.02, and ~ 6 μm for $0.06 \le x \le 0.25$ (Fig.2b). EDS analysis of the solid solutions shows the atomic fractions of the A-site (Na, Bi) and B-site (Ti, Sc) are close to their nominal values (Fig.2c and 2d), which further confirms the formation of a substantial solid solution between NBT and BS.

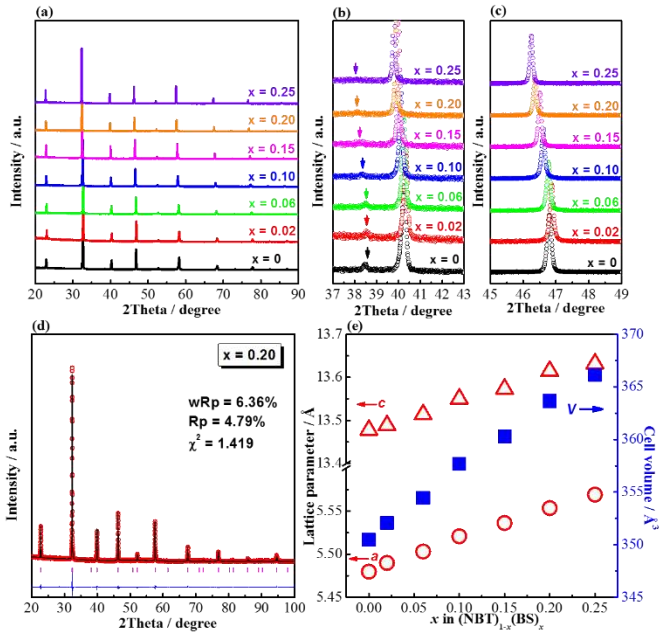

Fig. 1 (a) Room-temperature XRD patterns of $(NBT)_{1-x}(BS)_x$ ($0.00 \le x \le 0.25$) solid solutions; (b) an expanded view of the 2θ range between 37 and 43°. The arrows in the figure indicate the position of the superlattice reflection peak of the rhombohedral structure; (c) an expanded view of the 2θ range between 43 and 49°; (d) Rietveld refinement of the XRD pattern (x = 0.20 as an example). Hollow circles represent the observed pattern and the solid line shows the calculated fit. The reflection maker for the *R3c* structure is shown as vertical lines with the difference pattern below the diffraction pattern. The quality of fit is indicated in the figure. (e) Pseudo-cubic cell volume as a function of x. Error bars are within the symbols.

Table 1. Theoretical, experimental and relative densities of the sintered $(NBT)_{1-x}(BS)_x$ ($0 \le x \le 0.25$) ceramics.

Composition x	Density		
	Theoretical (g cm^{-3})	Experimental (g cm^{-3})	Relative (%)
0.00	6.00	5.72	95.3
0.02	6.04	5.77	95.6
0.06	6.09	5.91	97.0
0.10	6.15	5.76	93.6
0.15	6.23	5.86	93.9
0.20	6.30	6.06	96.3
0.25	6.38	6.04	94.7

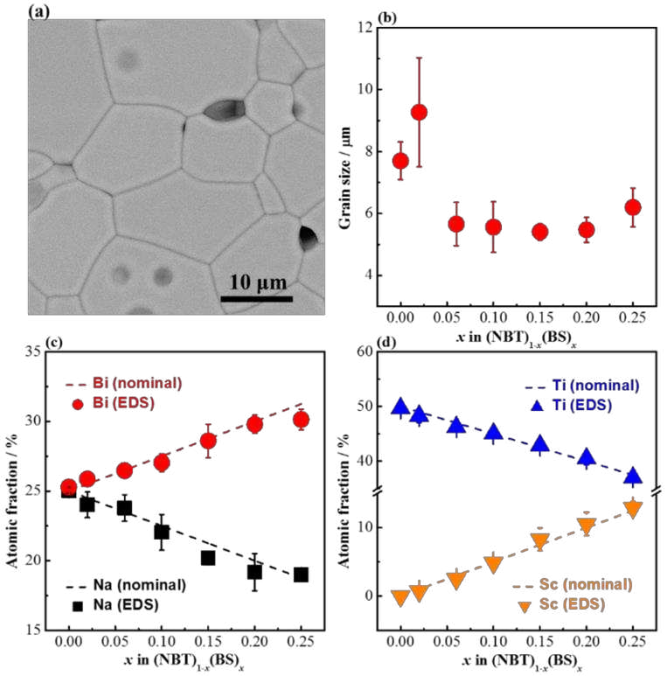

Fig.2 (a) A typical SEM micrograph of a thermally-etched surface of a $(NBT)_{1-x}(BS)_x$ ($0.00 \le x \le 0.25$) solid solution member ($x = 0.02$ as an example); (b) Average grain size as a function of x. Grain size of each composition was obtained by counting the number of grains across the diagonal. Error bars were from 5 micrographs. (c and d) Atomic fractions of the A-site (Na, Bi) and B-site (Ti, Sc) cations obtained from EDS, respectively. Data were collected from 5 randomly selected areas on polished surfaces without thermal etching.

Impedance spectra for selected members of the $(NBT)_{1-x}(BS)_x$ ($0.00 \le x \le 0.25$) solid solutions measured at 600 °C in flowing nitrogen, air and oxygen are shown in Fig.3. The Z* plot for NBT ($x = 0$), Fig.3a, shows three well-resolved ar°s, from high to low frequency, corresponding to responses from bulk, grain boundary and electrode effects, respectively. The high frequency response does not change with pO_2 and the electrode spike is more prominent in nitrogen, suggesting a predominant oxide-ion conduction mechanism for the bulk response of NBT. This is consistent with a previous study.[2] The M''-log$f$ spectroscopic plot, Fig.3b, suggests a characteristic frequency, $f_{max} > 1$ MHz for NBT. With BS incorporation, for example, $x = 0.02$, the Z* plot (Fig.3c) shows two less well-resolved arcs at high and intermediate frequency, along with an electrode spike at low frequency. The high frequency response, with an associated capacitance of ~ 1.0×10^{-10} F cm^{-1} corresponding to a relative permittivity of ~ 1100, does not change with pO_2, and the electrode spike is more prominent in nitrogen. The M''-log$f$ spectroscopic plot, Fig.3d, shows a single peak with a pO_2-independent f_{max} ~ 250 kHz. All this information suggests the bulk conduction for $x = 0.02$ is dominated by oxygen ions.

Similar features are observed on the Z* plot for $x = 0.15$ (Fig.3e), but with a larger impedance and a less pronounced electrode spike. The M''-log$f$ spectroscopic plot, Fig.3f, shows a pO_2 independent f_{max} ~ 50 kHz. With a further increase in BS content, i.e., $x = 0.25$, the Z* plot (Fig.3g) shows one distorted arc, which is largest when the sample is measured in flowing nitrogen and smallest when measured in oxygen, suggesting the presence of p- type electronic conduction. The electrode spike at low frequency can be still observed, although less apparent compared with NBT with lower BS content, and it is most prominent in nitrogen, suggesting the presence of oxide-ion conduction. The M''-log$f$ spectroscopic plot, Fig.3h, shows one single peak with f_{max} ~ 12 kHz for a sample measured in flowing oxygen and ~ 6.1 kHz in air and in flowing nitrogen. The capacitance associated with this single M'' peak is 7.9×10^{-10} F cm^{-1} corresponding to a relative permittivity of ~ 900, and therefore represents the bulk response. The pO_2-dependent impedance and f_{max}, along with the electrode spike, suggest a mixed ionic-electronic conduction mechanism for $x = 0.25$. Charge carriers are oxygen ions and holes.

For $x = 0$, the well-resolved impedance spectra were fitted by an equivalent circuit of three series-connected R-CPE elements to obtain the resistances R_b, R_{gb} and R_{tot} ($R_{tot} = R_b + R_{gb}$). For $0.02 \le x \le 0.25$, the bulk resistance was calculated from the M'' peak frequency and peak maximum[24] and the total resistance was obtained from the Z' intercept on Z* plots. This is to avoid large errors from equivalent circuit fitting due to the less well-resolved impedance responses from the bulk and grain boundary components. R_b and R_{tot} were converted to σ_b (= $1/R_b$) and σ_{tot} (= $1/R_{tot}$) and presented in Arrhenius plots, as shown in Fig.4. In general, σ_b and σ_{tot} decrease with increasing BS content but within the composition range between $0.06 \le x \le 0.20$ σ_b values are rather similar and do not show a clear trend with increasing x.

Activation energies (E_a) for σ_b and σ_{tot}, and the associated charge carriers, are listed in Table 2. For σ_b, E_a changes from 0.4 - 0.5 eV for $x = 0.00$ and 0.02, to 0.6 - 0.7 eV for $0.06 \le x \le 0.20$ and to ~ 0.9 eV for $x = 0.25$. For σ_{tot}, E_a for all compositions is 0.9 -1.2 eV. These values are much lower than ~ 1.7 eV for $NB_{0.51}T$ which shows typical type III behaviour.

The oxygen-ion transport number, t_{ion}, and bulk conductivity, σ_b, are plotted as a function of the BS content x in Fig.5. NBT-BS solid solutions show high t_{ion} (> 0.85) in a wide composition range $0.00 \le x \le 0.15$, and ~ 0.7 for $x = 0.20$ and 0.25. These values agree with the information obtained from the pO_2-dependence of the impedance (Fig.3). According to the previous classification of three types of electrical behaviour of NBT based on the magnitude of t_{ion}, the NBT-BS solid solutions with BS content $x \le 0.15$ belong to Type I behaviour and type II for $x = 0.20$ and 0.25. σ_b decreases with increasing x, reaching its minimum value ~ 10^{-5} S cm^{-1} at $x = 0.25$. Type III behaviour represented by $NB_{0.51}T$ with $t_{ion} < 0.1$and σ_b ~ 10^{-6} S cm^{-1} is not observed in NBT-BS solid solutions.

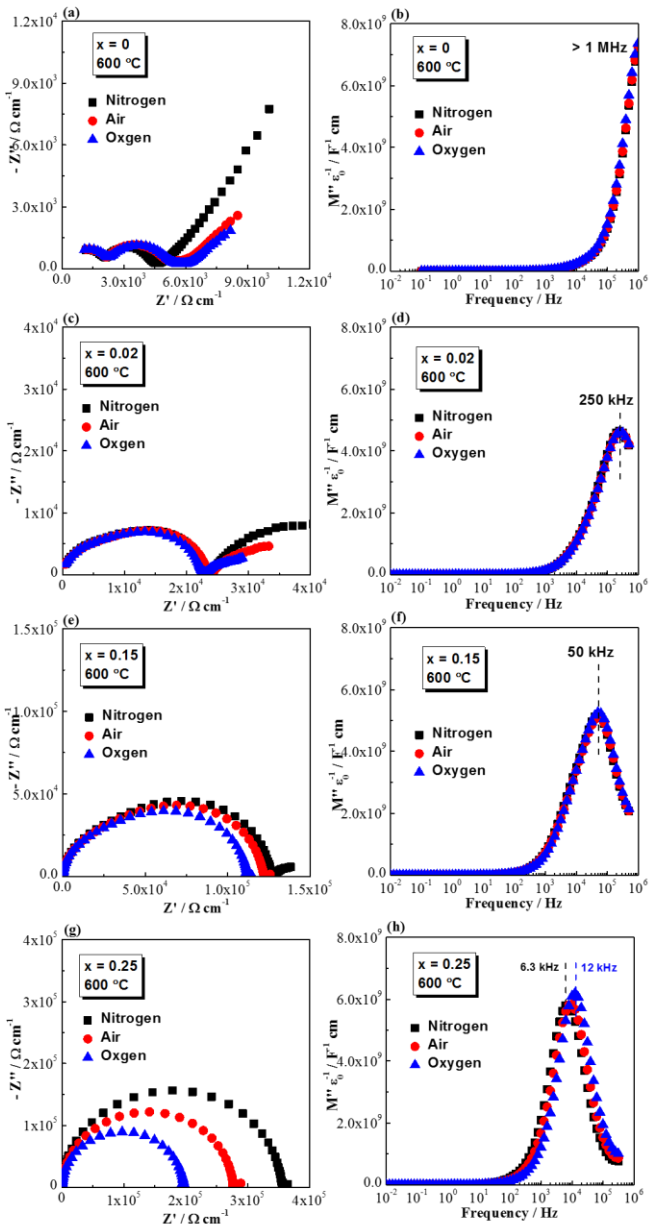

Fig.3 Impedance spectroscopy of $(NBT)_{1-x}(BS)_x$ ($0.00 \le x \le 0.25$) solid solutions at 600 °C in flowing nitrogen, air and oxygen in the frequency range from 1 MHz to 0.01 Hz. (a), (c) and (e): Z* plots for x = 0.02, 0.15 and 0.25, respectively. (b), (d) and (f): M''-log$f$ spectroscopic plots for x = 0.02, 0.15 and 0.25, respectively. The numbers inside each figure indicate the frequency at the M'' maxima.

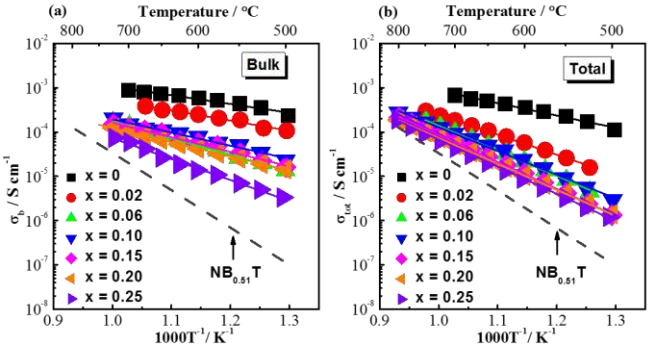

Fig.4 Arrhenius plots for (a) bulk conductivity, σ_b, and (b) total conductivity, σ_{tot}, of $(NBT)_{1-x}(BS)_x$ ($0.00 \le x \le 0.25$) solid solutions measured in air. Data for $NB_{0.51}T$ are also included for comparison (dash line in each figure).

Table 2 Activation energies, E_a, for the bulk conductivity and total conductivity of $(NBT)_{1-x}(BS)_x$ ($0.00 \le x \le 0.25$) solid solutions. Charge carriers are indicated in the parenthesis. Data for $NB_{0.51}T$ are included for comparison.

Composition x	E_a / eV	
	Bulk	Total
0	0.40 ± 0.03 (O^{2-})	0.90 ± 0.02 (O^{2-}, e)
0.02	0.46 ± 0.03 (O^{2-})	1.12 ± 0.02 (O^{2-}, h)
0.06	0.67 ± 0.02 (O^{2-})	1.07 ± 0.02 (O^{2-}, h)
0.10	0.60 ± 0.03 (O^{2-})	1.07 ± 0.01 (O^{2-}, h)
0.15	0.66 ± 0.03 (O^{2-})	1.22 ± 0.01 (O^{2-}, h)
0.20	0.64 ± 0.01 (O^{2-}, h)	1.17 ± 0.01 (O^{2-}, h)
0.25	0.87 ± 0.03 (O^{2-}, h)	1.23 ± 0.01 (O^{2-}, h)
$NB_{0.51}T$	1.69 ± 0.01 (e)	1.69 ± 0.01 (e)

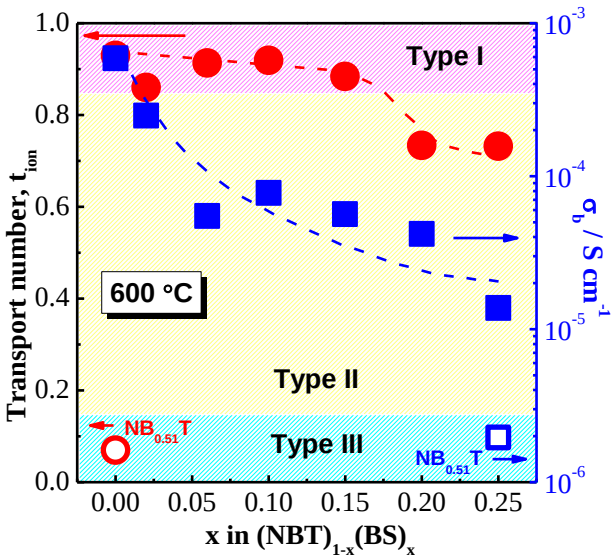

Fig.5 Oxygen-ion transport number, t_{ion}, and bulk conductivity, σ_b, at 600 °C as a function of composition factor x. t_{ion} and σ_b values for $NB_{0.51}T$ are included for comparison.

The permittivity-temperature (ε_r – T) profiles for the NBT-BS solid solutions are shown in Fig.6a. The permittivity maximum decreases from > 3000 for x = 0, to 2000 – 2500 for x = 0.02 and 0.06, to < 1500 for $x \geq 0.10$. The temperature where the permittivity reaches its maximum value, T_m, increases with increasing x, from ~ 325 °C for NBT, ~335 °C for x = 0.02, to 360 - 380 °C for $x \geq 0.06$. The ε_r – T data become flatter with increasing BS content, which agrees with previous reports.[15-17] Incorporation of BS into NBT also significantly changes the dielectric loss- temperature (tan δ – T) relationship, Fig.6b. NBT (x = 0) shows a sharp rise of tan δ with increasing temperature and tan δ exceeds 0.2 at ~ 350 °C. NBT-BS solid solutions show low tan δ (< 0.02) at 300- 400 °C and start to rise steeply at > 400 °C, exceeding 0.2 at 500 – 650 °C, which agrees with the definition of type II behaviour. Compared to the tan δ – T profile of $NB_{0.51}T$, it is also concluded that type III behaviour cannot be achieved in NBT-BS solid solutions.

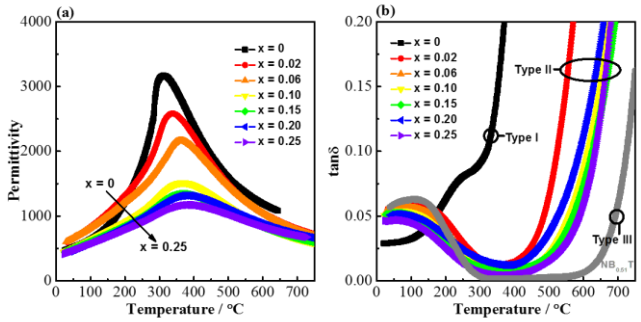

Fig.6. Dielectric spectroscopy of $(NBT)_{1-x}(BS)_x$ ($0 \leq x \leq 0.25$) solid solutions: (a) permittivity at 1 MHz versus temperature. (b) Dielectric loss (1 MHz) versus temperature. Data for $NB_{0.51}T$, showing type III behaviour, is also presented for comparison.

Discussion

Incorporation of BS into NBT decreases the bulk conductivity but the ionic transport number remains high (> 0.85) in a wide compositional range ($0 \leq x \leq 0.15$). The lowest transport number that can be obtained in the NBT-BS solid solutions is ~ 0.70 for x = 0.20 and 0.25, indicating that oxide-ion conduction cannot be fully suppressed, which is very different from the NBT-BA solid solutions where oxide-ion conduction can (within errors) be fully suppressed by ~ 7% BA incorporation (transport number ~ 0.03). Therefore, NBT-BS solid solutions can only present either Type I (predominant oxide-ion conduction) or Type II (mixed ionic-electronic conduction) behaviour based on the magnitude of bulk conductivity, transport number and dielectric loss-temperature profile. Furthermore, high levels of BS (i.e., x = 0.20 and 0.25) introduces p-type hole conduction into NBT, which is not observed in NBT-BA solid solutions. In the following sections, the defect chemistry and conduction mechanism(s) of the NBT-BS solid solutions are discussed; the possible reasons for the suppressed oxide-ion conductivity in NBT-BS solid solutions are proposed; the different electrical behaviours in NBT-BS, NBT-BA and NBT-BG solid solutions are compared and finally a new Type II behaviour in NBT-based materials is proposed.

Defect chemistry and conduction mechanism

When NBT forms a solid solution series with BS, there are two possible defect mechanisms:

(1) Ionic compensation, described by the following Kroger-Vink equation

$$A-site: Na_A^x + Bi_A^x + 2O_O^x + V_O^{\bullet\bullet} \xrightarrow{Bi_2O_3} Bi_{Na}^{\bullet\bullet} + Bi_A^x + 3O_O^x \quad (2a)$$

B-site: $$2Ti_{Ti}^x + 4\,O_O^x \xrightarrow{Sc_2O_3} 2Sc_{Ti}' + 3O_O^x + V_O^{\bullet\bullet} \quad (2b)$$

(2) Electronic compensation, described by

A-site:

$$Na_A^x + Bi_A^x + 2O_O^x + \frac{1}{2}O_2(g) \xrightarrow{Bi_2O_3} Bi_{Na}^{\bullet\bullet} + Bi_A^x + 2e^- + 3O_O^x \quad (3a)$$

B-site:

$$2Ti_{Ti}^x + 4\,O_O^x \xrightarrow{Sc_2O_3} 2Sc_{Ti}' + 3O_O^x + 2h^{\bullet} + \frac{1}{2}O_2(g) \quad (3b)$$

Both mechanisms lead to an overall reaction, described by

Overall:

$$Na_A^x + Bi_A^x + 2Ti_{Ti}^x + 6O_O^x \xrightarrow{2BiScO_3} Bi_{Na}^{\bullet\bullet} + Bi_A^x + 2Sc_{Ti}' + 6O_O^x. \quad (3)$$

In the above equations, the subscript A denotes the disorder of the Na and Bi ions on the A-site of the NBT lattice. Both mechanisms are considered as a 'stoichiometric' doping mechanism without creating any additional charge carriers. However, due to a small amount of Bi_2O_3-loss during ceramic processing, oxygen vacancies are generated according to

$$2Bi_{Bi}^x + 3O_O^x \rightarrow 2V_{Bi}''' + 3V_O^{\bullet\bullet} + Bi_2O_3. \quad (4)$$

As these ceramics are prepared by furnace cooling, uptake of oxygen gas on cooling may occur to fill the oxygen vacancies and generate holes, given by

$$V_O^{\bullet\bullet} + \frac{1}{2}O_2(g) \rightarrow O_O^x + 2h^{\bullet}. \quad (5)$$

For nominally stoichiometric NBT ($NB_{0.50}T$), our previous study[2] using a combination of impedance spectroscopy in various pO_2's, electromotive force (EMF) and ^{18}O Time-of-Flight Secondary Ion Mass Spectroscopy (ToF SIMS) revealed the electrical conduction in $NB_{0.50}T$ is dominated by migration of oxygen ions (or oxygen vacancies). Oxygen ions are highly mobile in NBT and result in a high ionic conductivity (approaching 10^{-3} S cm^{-1} at 600 °C) although the charge carrier concentration is extremely low (< 0.1%).[25] p-type hole conduction described by Eq.5 may also exist but as the ionic conductivity is very high the contribution from hole conduction to the overall conduction is negligible.

For the NBT-BS solid solutions, impedance spectroscopy under various pO_2's (Fig.3a-f) and EMF transport number measurements (Fig.5) show a pO_2-independent bulk response and a high ionic transport number (> 0.85) for $x \leq 0.15$, suggesting the bulk conduction is predominately oxygen ions. Therefore, the defect chemistry described by Eq.4 is the major mechanism for the bulk electrical conduction. With higher BS levels of x = 0.20 and 0.25, a pO_2-dependent impedance response (Fig.3g-h, x = 0.25 as an example) and a lower transport number (~ 0.7) suggests mixed ionic-electronic conduction behaviour. The defect chemistry described in both Eq.4 and 5 contribute to the electrical conduction in these high BS content solid solutions.

Suppression of oxide-ion conduction by BS incorporation

1) Oxide ion conduction for $x \leq 0.15$

As discussed above, the bulk conduction of $(NBT)_{1-x}(BS)_x$ solid solutions with $x \leq 0.15$ is predominately oxygen ions. For a single type of charge carrier, the electrical conductivity is determined by σ =

$c \bullet q \bullet \mu$, where c, q and μ are the concentration, charge and mobility of the charge carriers, respectively. As the oxide-ion conductivity of NBT is suppressed by BS incorporation, there is either a decrease in the concentration and/or a decrease in the mobility of oxygen vacancies.

Oxygen vacancies in the NBT-BS solid solutions are only generated by very low levels of Bi_2O_3-loss during ceramic processing. Given a 0.17-0.33% Bi_2O_3-loss[25] for all the compositions, the oxygen deficiency varies from 0.0025-0.005 for NBT (x = 0.00) to 0.0030-0.0057 for x = 0.15. Such low level of oxygen deficiency (and therefore the oxygen vacancy concentration) is not completely controllable and should occur at a randomly low level. Arrhenius plots (Fig.5) and the conductivity-composition relationship (Fig.6) both show no systematic trend with x in the composition range between x = 0.06 and 0.20. Therefore, a slight variation of the oxygen vacancy concentration may be possible. However, it should be noted that all the σ_b values for x > 0.00 are lower than σ_b for x = 0.00, indicating the random change of oxygen vacancy concentration is not the dominant factor for the suppressed conductivity. The mobility of oxygen vacancies plays a much more important role in the oxide-ion conduction in the NBT-BS solid solutions.

From an average structure point of view, oxide-ion conductivity in a perovskite is usually predicted by the Goldschmidt tolerance factor t[26], the lattice free volume V_{sf} [20] and the critical radius r_C[21]. Details of the definition and calculation of the above empirical parameters can be found in ref.9. Previous studies on a large number of oxide-ion conductors crystallising in the perovskite structure show that the highest conductivity can be achieved with t ~ 0.96,[20] and that large V_{sf} and r_C are beneficial for migration of oxygen ions. The calculated t, V_{sf} and r_C values for the NBT-BS solid solutions are listed in Table 3. With increasing BS content, t decreases and approaches the optimum value 0.96, furthermore, both V_{sf} and r_C increase. These are all beneficial to oxide-ion conduction in perovskites, and cannot explain the suppressed conductivity by BS incorporation. Other factor(s) as opposed to the average structure dominate(s) the electrical conductivity of NBT-BS solid solutions.

Table 3. Tolerance factor t, specific free volume V_{sf}, and critical radius r_C of $(NBT)_{1-x}(BS)_x$ ($0 \le x \le 0.15$) solid solutions.

x	t	V_{sf}	r_C (Å)
0	0.9841	0.2012	0.9074
0.02	0.9827	0.2033	0.9084
0.06	0.9800	0.2074	0.9105
0.10	0.9773	0.2115	0.9125
0.15	0.9739	0.2166	0.9150

In perovskite-based oxide-ion conductors, the oxygen ion migration is through a saddle point which is a triangle formed by two A-site cations and one B-site cation.[10] Results from first-principles calculations on NBT showed the energy barriers for oxygen ion migration are 0.22, 0.6-0.85 and 1.0-1.3 eV for Bi-Bi-Ti, Na-Bi-Ti and Na-Na-Ti saddle points, respectively. The energy barriers are related to the polarisability of the ions at the saddle points: Bi^{3+} has the highest polarisability (α_{Bi} = 6.12 Å^3)[27] Na^+ the lowest (α_{Na} = 1.80 Å^3)[27] and Ti^{4+} in the middle (α_{Ti} = 2.93 Å^3)[27]. Experimentally there is no evidence for long-range ordering of Na and Bi on A-site, therefore the Na-Bi-Ti saddle points are considered as the rate-limiting step in the overall oxygen ion migration in NBT.[4, 9] Incorporation of BS into NBT introduces Bi-Bi-Sc, Na-Bi-Sc and Na-Na-Sc saddle points. The polarisability of Sc^{3+}, α_{Sc} = 2.81 Å^3,[27] is slightly lower than α_{Ti}. The energy barriers for oxygen ion migrating through the Sc-containing saddle points should be quite similar to the values for Ti-containing saddle points. On the other hand, there is no evidence for the ordering of the A-site cations with BS incorporation: no additional XRD peaks (Fig.1) were observed. Therefore, the Na-Bi-Ti(Sc) saddle points are still considered to dominate the energy barrier for oxygen ion migration in NBT-BS solid solutions. The slightly lower polarisability of Sc^{3+} cannot be the determinant factor for the suppressed conductivity.

The decreased mobility of charge carriers can originate from trapping of oxygen vacancies. First-principles calculations[12] showed that trapping of oxygen vacancies by B-site acceptor dopants significantly increases the oxygen migration barrier. Our previous experimental studies also showed the strong tendency of trapping between B-site acceptor dopants and oxygen vacancies.[6, 9] In the NBT-BS solid solutions, Sc'_{Ti} can trap $V_O^{\bullet\bullet}$ to form the defect complex$(Sc'_{Ti} - V_O^{\bullet\bullet})^{\bullet}$, which reduces the mobility of $V_O^{\bullet\bullet}$, and thus suppresses the oxide-ion conductivity. Goff *et al.*[28] studied the defect structure of $(ZrO_2)_{1-x}(Y_2O_3)_x$ ($0.10 \le x \le 0.24$) single crystals by neutron and X-ray diffraction and proposed the acceptor dopants Y'_{Zr} can form static aggregates with the host ion Zr^{4+}. With increasing x, the number of static aggregates increases to block the migration of $V_O^{\bullet\bullet}$, consequently reduces the mobility of $V_O^{\bullet\bullet}$ and the ionic conductivity. This mechanism requires a high concentration of acceptor dopants, i.e., > 20% Y'_{Zr}, to block the charge carrier. In NBT-BS solid solutions, suppressed conductivity is observed even for 2% Sc'_{Ti} on the Ti-site. Our previous study on NBT-BA solid solutions showed that only 7% Al'_{Ti} on the B-site can fully eliminate the oxide ion conduction and decrease the conductivity by ~ 3 orders of magnitude at 600 °C. Therefore, trapping between B-site acceptor dopants and oxygen vacancies may be a more plausible explanation for the reduced mobility of charge carriers in NBT-BS solid solutions.

The suppressed ionic conductivity in NBT-BS solid solutions further supports our previous findings that a Bi-rich A-site environment is not necessarily good for oxide-ion conduction. Trapping of oxygen vacancies by B-site acceptor-dopants plays a much more important role in the oxide-ion conduction of the NBT-based materials compared to the enlarged channel for oxygen migration due to lattice expansion.

2) Mixed conduction for x = 0.20 and 0.25

NBT-BS solid solutions with high BS level (x = 0.20 and 0.25) show mixed ionic-electronic (p-type) conduction behaviour with an ionic transport number ~ 0.7. Additional to the trapping effect between Sc'_{Ti} and$V_O^{\bullet\bullet}$, suppression of ionic conduction may also originate from filling of oxygen vacancies by oxygen gas during furnace cooling (Eq.5), which reduces the charge carrier concentration for ionic conduction. Creation of holes introduces p-type electronic conduction into the material and starts to have a visible effect to the overall conductivity. It is worth mentioning that as the p-type

electronic conduction only contributes to ~30% of the total conduction, the amount of oxygen gas uptake should be very small.

In summary, we propose the composition-conductivity ($\sigma_b - x$) relationship in NBT-BS solid solutions can be divided into two composition regions: a) $0.00 \le x \le 0.15$, predominant oxide-ion conduction and b) $x \ge 0.20$, mixed ionic –electronic conduction. The $\sigma_b - x$ relationship is a competing effect from lattice expansion, which enlarges the channel for oxygen ion migration, and trapping between B-site acceptor Sc'_{Ti} and oxygen vacancy $V_O^{\bullet\bullet}$, which decreases the mobility of charge carriers. As illustrated in Fig.7, the lattice expansion is beneficial to the oxide-ion conduction to enhance the conductivity (green dash line); however, trapping between Sc'_{Ti} and $V_O^{\bullet\bullet}$ is detrimental to the oxide-ion conduction and decreases the conductivity (green dot line). The trapping effect plays a more important role on the conductivity than the lattice expansion, therefore the overall ionic conductivity shows a general decreasing trend with increasing x (solid green line) but experimentally σ_b may deviate from the solid green line due to the random and uncontrollable oxygen vacancy concentration. Hole conduction (described by Eq.5) may exist for all compositions but the p-type electronic conductivity is very low (grey solid line). For $0.00 \le x \le 0.15$, contribution from hole conduction is negligible because the ionic conductivity for these compositions is high; for $x \ge 0.20$, ionic conduction is further suppressed by the trapping effect so p-type hole conduction starts to contribute to the overall electrical conductivity and gives rise to the mixed conduction behaviour.

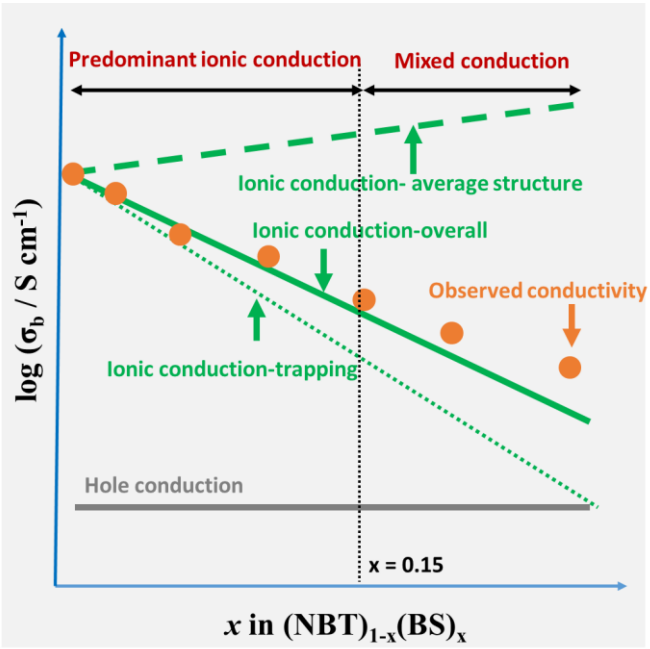

Fig.7 A schematic illustration of the composition- bulk conductivity relationship in NBT-BS solid solutions.

Trapping ability- ionic size effect

The bulk conductivity-composition ($\sigma_b - x$) relationship in NBT-BA, BG and BS solid solutions are compared in Fig. 8a. σ_b for all three series decreases with increasing x. NBT-BA and NBT-BS solid solutions show the most and least dramatic decrease in conductivity with increasing x, respectively. Ionic transport number, t_{ion}, for NBT-BA solid solutions decreases continuously with increasing x, from close to 1 for $x = 0.00$ to close to zero for $x = 0.07$; t_{ion} for NBT-BS solid solutions remains ~ 0.9 for $x \le 0.15$ and decreases to ~ 0.7 for $x = 0.20$ and 0.25, Fig.8b. As discussed in 4.2, trapping of oxygen vacancies by B-site acceptor dopants is the major reason for the suppressed conductivity in these solid solutions, Fig.8a and 8b suggest a significant difference in the ability of $V_O^{\bullet\bullet}$ trapping between Sc'_{Ti} and Al'_{Ti}, which may originate from an ionic size effect.

Andersson *et al.*[30] reported that in acceptor-doped ceria, the preferred location of an oxygen vacancy depends on the ionic size of the dopant: if the dopant ion is smaller or similar to the host ion, an oxygen vacancy prefers to locate on the first nearest neighbour (1NN) site of the dopant ion; if the dopant ion is considerably larger than the host ion, oxygen vacancies prefer to locate on the second nearest neighbour (2NN) site of the dopant. As illustrated in Fig.8b, Al^{3+} is much smaller than Ti^{4+} and Ga^{3+} is only slightly larger than Ti^{4+} so the oxygen vacancy would prefer the 1NN site for Al'_{Ti} or Ga'_{Ti}. Al'_{Ti} or Ga'_{Ti} and $V_O^{\bullet\bullet}$ are in close proximity and this results in a high attractive electrostatic force. On the contrary, as Sc^{3+} is much larger than Ti^{4+}, 2NN sites of Sc'_{Ti} is favoured for $V_O^{\bullet\bullet}$ and consequently result in a weak attractive electrostatic force between Sc'_{Ti} and $V_O^{\bullet\bullet}$.

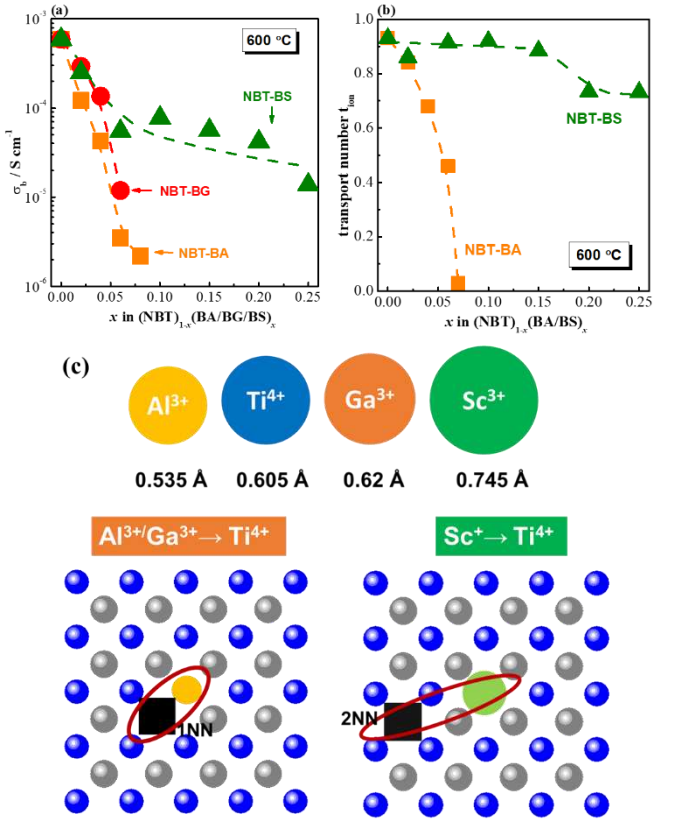

Fig.8 (a) Bulk conductivity-composition and (b) transport number-composition relationship of NBT-BA, BG and BS solid solutions at 600 °C. Data for NBT-BA and NBT-BG are from ref.9 and 29, respectively. (c) A schematic view of the dopant ionic size effect on the preferred site of an oxygen vacancy with the respect to the dopant ions.

The weaker ability of trapping oxygen vacancies by larger B-site acceptor dopants in NBT is also supported by our previous findings that at the same oxygen vacancy concentration, Sc-doped NBT shows higher bulk conductivity than Ga- or Al-doped NBT.[6] In NBT, the TiO_6 octahedra are heavily tilted due to A-site Na/Bi disorder, which results in different local configurations to benefit oxygen ion migration. Therefore, the mobility of oxygen ions in NBT is exceptional high and shows high conductivity for very low charge carrier concentration. A small change in the local structure can result in a significant change in the mobility of oxygen ions, and consequently the oxide-ion conductivity. This is a possible reason why the oxide-ion conduction in NBT is sensitive to the type of acceptor dopants.

Whether the weak trapping ability of large acceptor dopants in NBT-based materials can be expanded to a wider range of oxide-ion conductors, i.e., fluorites, melilite, apatite, etc, should be considered with caution. Although it is generally accepted that dopants with sizes close to the host ion often introduce higher ionic conductivity than those with very different size compared with the host ion, the dopant size effect is still controversial even in the best known fluorite-type oxide-ion conductors, i.e., acceptor-doped CeO_2 and acceptor-doped ZrO_2. For example, in acceptor-doped CeO_2 systems, the highest conductivity is achieved in Nd-doped CeO_2[31] where Nd^{3+} (1.11 Å, 8-fold coordination) is much larger than Ce^{4+} (0.97 Å, 8-fold coordination) whereas in ZrO_2 system, the highest conductivity is obtained for Sc-doped ZrO_2[32] where Sc^{3+} (0.87 Å, 8-fold coordination) is closest to the size of Zr^{4+} (0.84 Å, 8-fold coordination). In these heavily doped fluorites, alternative explanations to the trapping effect may be more plausible.[28] In melilite- or apatite-type oxide-ion conductors, the ionic conduction is usually via an oxygen interstitial mechanism.[33, 34] How the acceptor-dopants trap oxygen vacancies in these structures still needs investigation.

Revisit the three types of electrical behaviour of NBT

We have previously classified the electrical behaviour of NBT-based materials into three types based on the magnitude of t_{ion}, σ_b and tan δ at elevated temperatures, in which Type II NBT usually shows a t_{ion} ~ 0.5. For NBT-BS solid solutions in the compositional range between x = 0.02 and 0.15, although σ_b and tan δ show typical Type II behaviour, t_{ion} remains high (~ 0.9), indicating the tan δ – T relationship depends on the magnitude of conductivity but not on the conduction mechanism. A high t_{ion} does not necessarily lead to a high tan δ, and vice versa. Therefore, here we propose a new Type II behaviour of NBT-based material, which shows high t_{ion} but intermediate σ_b and tan δ. Caution should therefore be taken when predicting the conduction mechanism based on tan δ – T profiles for NBT-based materials.

Conclusions

$(NBT)_{1-x}(BS)_x$ ($0.00 \le x \le 0.25$) solid solutions were prepared by solid state reaction and their electrical properties studied by *ac* impedance spectroscopy and electromotive force transport number measurements. The bulk conductivity decreases with increasing BS incorporation but the oxide-ion transport number remains high (> 0.85) over a wide compositional range $0 \le x \le 0.15$ and drops to ~ 0.7 for $x \ge 0.20$. Therefore, NBT-BS solid solutions can only present either predominant oxide-ion conduction (Type I) or mixed ionic-electronic conduction (Type II) behaviour. Predominant electronic conduction (Type III) behaviour is not observed in NBT-BS solid solutions even at its upper solution limit (25%). Oxide-ion conduction cannot be fully eliminated by BS incorporation, which is in contrast from a previous study where ~7% $BiAlO_3$ (BA) incorporation can fully suppress the oxide-ion conduction in NBT. The conductivity-composition relationships of NBT-BS solid solutions is attributed to a competing effect between lattice expansion and trapping of oxygen vacancies by B-site Sc acceptor dopants. Comparison of NBT-BS with NBT-BA and NBT-BG solid solutions reveal small B-site acceptor ions are more effective in trapping oxygen vacancies and consequently more effective in suppressing oxide-ion conduction in the NBT lattice. This makes BA and BG more useful as solid solution end members for NBT-based materials for high temperature dielectric applications due their much lower dielectric loss.

Conflicts of interest

There are no conflicts to declare.

Acknowledgements

We thank the EPSRC for funding EP/L027348/1.

References

1 J. Zhang, Z. Pan, F. Guo, W. Liu, H. Ning, Y. B. Chen, M. Lu, B. Yang, J. Chen, S. Zhang, X. Xing, J. Rödel, W. Cao and Y. Chen, Nat. Commun., 2015, 6, 6615.
2 A. Mahajan, H. Zhang, J. Wu, E. Venkata Ramana, M. J. Reece and H. Yan, J. Phys. Chem. C, 2017, 121, 5709.
3 J. Wu, A. Mahajan, L. Riekehr, H. Zhang, B. Yang, N. Meng, Z. Zhang and H. Yan, Nano Energy, 2018, 50, 723.
4 J. Li, F. Li, Z. Xu and S. Zhang, Adv. Mater., 2018, 30, 1802155.
5 M. Li, M. J. Pietrowski, R. A. De Souza, H. Zhuang, I. M. Reaney, S. N. Cook, J. A. Kilner and D . C. Sinclair, Nat. Mater., 2014, 13, 31.
6 F. Yang, M. Li, L. Li, P. Wu, E. Pradal-Velázquez and D. C. Sinclair, J. Mater. Chem. A, 2018, 6, 5243.
7 L. Li, M. Li, H. Zhang, I. M. Reaney and D. C. Sinclair, J. Mater. Chem. C, 2016, 4, 5779.
8 M. Li, H. Zhang, S. N. Cook, L. Li, J. A. Kilner, I. M. Reaney and D. C. Sinclair, Chem. Mater., 2015, 27, 629.
9 F. Yang, P. Wu and D. C. Sinclair, J. Mater. Chem. C, 2017, 5, 7243.
10 M. S. Islam, J. Mater. Chem., 2000, 10, 1027.
11 J. A. Dawson, H. Chen and I. Tanaka, J. Mater. Chem. A, 2015, 3, 16574.
12 X. He and Y. Mo, Phys. Chem. Chem. Phys., 2015, 17, 18035.
13 K. Meyer and K. Albe, J. Mater. Chem. A, 2017, 5, 4368.
14 L. Koch, S. Steiner, K. Meyer, I. Seo, K. Albe and T. Frömling, J. Mater. Chem. C, 2017, 5, 8958.
15 P. Marchet, E. Boucher, V. Dorcet and J. P. Mercurio, J. Euro. Ceram. Soc., 2006, 26, 3037.
16 E. Boucher, P. Marchet and J. P. Mercurio, J. Phys. IV France, 2005, 128, 3.
17 H. Nagata and T. Takenaka, Jpn. J. Appl. Phys., 1997, 36, 6055.
18 R. D. Shannon, Acta Crystallog. A, 1976, 32, 751.
19 G. O. Jones and P. A. Thomas, Acta Crystallogr. B, 2002, 58, 168.
20 H. Hayashi, H. Inaba, M. Matsuyama, N. G. Lan, M. Dokiya and H. Tagawa, Solid State Ionics, 1999, 122, 1.
21 J. A. Kilner and R. J. Brook, Solid State Ionics, 1982, 6, 237.

22 A. C. Larson and R. B. Von Dreele, General Structure Analysis System (GSAS). Los Alamos National Laboratory Report LAUR 1994, pp. 86-748.
23 B. H. Toby, J. Appl. Crystallogr., 2001, 34, 210.
24 F. Yang, M. Li, L. Li, P. Wu, E. Pradal-Velázquez, H. K. Pearce and D. C. Sinclair, J. Mater. Chem. C, 2018, 6, 9258.
25 M. Li, L. Li, J. Zang and D. C. Sinclair, Appl. Phys. Lett., 2015, 106, 102904.
26 V. M. Goldschmidt, T. Barth, G. Lunde and W. Zachariasen, Pt. VII Skrifter Norske Videnskabs-Akademi, Oslo, 1926, p. 117.
27 N. M. Grimes and R. W. Grimes, J. Phys.: Condens. Matter, 1998, 10, 3029.
28 J. P. Goff, W. Hayes, S. Hull, M. T. Hutchings and K. N. Clausen, Phys. Rev. B, 1999, 59, 14202.
29 P. Wu, PhD Thesis, University of Sheffield, 2018.
30 D. A. Andersson, S. I. Simak, N. V. Skorodumova, I. A. Abrikosov and B. Johansson, Proc. Natl. Acad. Sci. USA, 2006, 103, 3518.
31 S. Omar, E. D. Wachsman, J. L. Jones and J. C. Nino, J. Am. Ceram. Soc., 2009, 92, 2674.
32 O. Yamamoto, Y. Arachi, H. Sakai, Y. Takeda, N. Imanishi, Y. Mizutani, M. Kawai and Y. Nakamura, Ionics, 1998, 4, 403.
33 H. J. Park, T. Kim, C. Kwak, D. W. Jung, S. Lee and K. H. Lee, J. Power Sources, 2015, 275, 884.
34 H. Zhang, F. Li, J. Jin, Q. Wang and Y. Sun, Solid State Ionics, 2008, 179, 1024.

